### Title

Multiphase Buffering by Ammonia Sustains Sulfate Production in Atmospheric Aerosols




### Journal

AGU Advances, 5(4)

### ISSN

2576-604X



### Authors

Zheng, Guangjie

Su, Hang

Andreae, Meinrat O

et al.



### Publication Date

2024-08-01

### DOI

10.1029/2024av001238

AGU ADVANCING EARTH AND SPACE SCIENCES

AGU Advances

RESEARCH ARTICLE
10.1029/2024AV001238

# Multiphase Buffering by Ammonia Sustains Sulfate Production in Atmospheric Aerosols

**Guangjie Zheng[1,2], Hang Su[3], Meinrat O. Andreae[1,4], Ulrich Pöschl[1], and Yafang Cheng[1]**

[1]Max Planck Institute for Chemistry, Mainz, Germany, [2]State Key Joint Laboratory of Environmental Simulation and Pollution Control, School of Environment, Tsinghua University, Beijing, China, [3]Key Laboratory of Atmospheric Environment and Extreme Meteorology, Institute for Atmospheric Physics, Chinese Academy of Science, Beijing, China, [4]Scripps Institution of Oceanography, University of California San Diego, San Diego, CA, USA

**Peer Review** The peer review history for this article is available as a PDF in the Supporting Information.

**Key Points:**

- A characteristic buffering time is proposed to evaluate the competing effects of multiphase buffering and acidification on aerosol pH
- For most areas, the buffer effect can overwhelm acidification and sustain sulfate production from high pH-favored multiphase reactions

**Supporting Information:**

Supporting Information may be found in the online version of this article.

**Correspondence to:**

Y. Cheng and H. Su,
yafang.cheng@mpic.de;
suhang@mail.iap.ac.cn

**Citation:**

Zheng, G., Su, H., Andreae, M. O., Pöschl, U., & Cheng, Y. (2024). Multiphase buffering by ammonia sustains sulfate production in atmospheric aerosols. *AGU Advances*, *5*, e2024AV001238. https://doi.org/10.1029/2024AV001238

Received 4 MAR 2024
Accepted 2 JUL 2024

**Author Contributions:**

**Conceptualization:** Guangjie Zheng, Hang Su, Yafang Cheng
**Data curation:** Guangjie Zheng, Hang Su, Meinrat O. Andreae, Ulrich Pöschl, Yafang Cheng
**Formal analysis:** Guangjie Zheng, Hang Su, Meinrat O. Andreae, Ulrich Pöschl, Yafang Cheng
**Funding acquisition:** Yafang Cheng
**Investigation:** Guangjie Zheng, Hang Su, Meinrat O. Andreae, Ulrich Pöschl, Yafang Cheng
**Methodology:** Guangjie Zheng, Hang Su, Yafang Cheng
**Software:** Guangjie Zheng



**Abstract** Multiphase oxidation of sulfur dioxide ($SO_2$) is an important source of sulfate in the atmosphere. There are, however, concerns that protons produced during $SO_2$ oxidation may cause rapid acidification of aerosol water and thereby quickly shut down the fast reactions favored at high pH. Here, we show that the sustainability of sulfate production is controlled by the competing effects of multiphase buffering and acidification, which can be well described by a characteristic buffering time, $\tau_{buff}$. Both GEOS-Chem simulations and observations show that globally, $\tau_{buff}$ is long enough (days) to sustain sulfate production over most populated regions, where the acidification of aerosol water is counteracted by the strong buffering effect of $NH_4^+/NH_3$. Our results highlight the importance of anthropogenic ammonia emissions and pervasive human influences in shaping the chemical environment of the atmosphere.

**Plain Language Summary** Aerosol acidity largely regulates the chemistry of atmospheric particles and their environmental effects. Understanding the role of proton ($H^+$) generating reactions is thus a major challenge in understanding and modeling of atmospheric multiphase chemistry. Here, by accounting for the competing effects of multiphase buffering and acidification, we develop a new method to evaluate the role of these reactions on aerosol pH and pH-sensitive reactions. We find that over most populated regions, the buffering effect is so strong that it overwhelms the influence of acidification and sustains sulfate production from high pH-favored multiphase reactions. Our results highlight the importance of anthropogenic ammonia emissions in buffering the acidity of aerosol particles and in regulating the change of atmospheric compositions via multiphase reactions.

## 1. Introduction

Multiphase reactions are important sources of secondary aerosols and fine particulate matter in the atmosphere, influencing air quality, climate, and human health (Akimoto & Hirokawa, 2020; Seinfeld & Pandis, 2016; Su et al., 2020; G. Zheng et al., 2020; G. J. Zheng et al., 2015). Acidity is a key parameter in multiphase reactions, affecting gas-liquid partitioning and reaction rates (Jang et al., 2002; Pye et al., 2020; Tilgner et al., 2021; G. Zheng et al., 2020). The impact of acidity is particularly strong in sulfate formation (Cheng et al., 2016; Seinfeld & Pandis, 2016), a major component of fine particulate matter in the atmosphere (Snider et al., 2016). Elevated aerosol pH above 4.5 favors aqueous sulfate formation via $SO_2$-$O_3$ and $SO_2$-$NO_2$ pathways, while low pH favors the reaction via $SO_2$-$O_2$ catalyzed by transition metal ions (TMI) (Cheng et al., 2016; Seinfeld & Pandis, 2016). The major oxidation pathways may vary, with $SO_2$-$NO_2$, $SO_2$-$O_3$, $SO_2$-TMI, and $SO_2$-$H_2O_2$ reactions alternatively dominant in different regions depending on the prevailing aerosol pH and precursor concentrations (Keene et al., 1998; Tao et al., 2020).

Because the formation of sulfate is always accompanied by proton ($H^+$) production, there is an arising concern whether the fast reactions favored at high pH can maintain their reaction rates upon acidification (Alexander et al., 2005; Angle et al., 2021; Keene et al., 1998; Laskin et al., 2003; T. Liu et al., 2021; Pye et al., 2020; Tilgner et al., 2021; W. Wang et al., 2021). The time scale of acidification is thus important in predicting the total amount of sulfate produced and its environmental and climate effects. For example, changing the acidification time scale from ~1 hr to ~1 day would increase the contribution of sea salt chemistry to the global sulfate burden from 1% to 13% (Alexander et al., 2005; Angle et al., 2021; Chameides & Stelson, 1992; Laskin et al., 2003; H. Liao et al., 2004; Salter et al., 2016). In the polluted boundary layer, a recent comprehensive review on aerosol acidity and multiphase chemistry (Tilgner et al., 2021) suggested that the acidification can be so efficient that haze

**Supervision:** Hang Su, Yafang Cheng
**Validation:** Guangjie Zheng
**Visualization:** Guangjie Zheng
**Writing – original draft:** Guangjie Zheng, Hang Su, Yafang Cheng
**Writing – review & editing:** Guangjie Zheng, Hang Su, Meinrat O. Andreae, Ulrich Pöschl, Yafang Cheng

particles with initial pH above ∼4 will be acidified to as low as pH ∼1 within 10 s. However, G. Zheng et al. (2020) found that ammonia could buffer aerosol pH in large areas of the continent, implying a slow acidification process. Observations also show that with fast sulfate production under polluted conditions in the North China Plain, aerosol pH can be maintained at > 4–6 for hours to days depending on meteorological conditions (J. Ding et al., 2019; Shi et al., 2017). So far, it is still not clear how efficiently the buffer effect can compete with acidification and sustain the pH-sensitive reactions in sulfate production.

## 2. Materials and Methods

### 2.1. Calculating the Temporal Evolution of Aerosol pH Upon Acidification

#### 2.1.1. Simulation of the Actual Buffered Aerosols

To elucidate the temporal evolution of aerosol pH upon acid production by sulfate-forming reactions in polluted regions, we take as an example the severe winter haze conditions in the North China Plain (referred to the NCP scenario hereinafter) (Cheng et al., 2016; Tilgner et al., 2021; G. Zheng et al., 2020). Briefly, sulfate production works like adding sulfuric acid to the system, namely:

$$n_{\mathrm{acid}} = 2\,\Delta\left[\mathrm{SO}_4^{2-}\right] = 2\int P_{\mathrm{SO4}}\mathrm{d}t \tag{1}$$

where $n_{\mathrm{acid}}$ is the amount of equivalent strong monoacid added to the system in unit of μmol $m^{-3}$, $\Delta[SO_4^{2-}]$ is the total generated sulfate, and $P_{SO4}$ is the sulfate production rate in unit of in unit of μmol $m^{-3}$ $s^{-1}$. The $P_{SO4}$ is a function of aerosol pH, and the aerosol pH is a function of total sulfate. The dependence of $P_{SO4}$ on pH is calculated explicitly as parameterized in Cheng et al. (2016) (Figure S1 in Supporting Information S1), while the influence of ionic strength (T. Liu & Abbatt, 2021; T. Liu et al., 2021; T. Liu et al., 2020) and other potential mechanisms (Chen et al., 2022; W. Wang et al., 2021) etc. are discussed Section S1 and Figures S2–S3 in Supporting Information S1. The pH under different total sulfate concentrations can be estimated by the ISORROPIA model (Fountoukis & Nenes, 2007). Therefore, the aerosol pH change due to sulfate formation can be calculated iteratively by accounting for the newly formed sulfate in the ISORROPIA inputs, as briefly detailed below.

The initial conditions (i.e., at reaction time $t = 0$) of aerosol compositions followed the NCP scenario in Zheng et al. (2020) (Table S1 in Supporting Information S1), which are kept constant except the sulfate concentrations in the following calculations. The initial pH is estimated by the ISORROPIA model under this condition. Afterward, the sulfate and pH evolutions are calculated iteratively with a time step $\Delta t$. Note that the $\Delta t$ is the actual time interval used in model simulations as a surrogate of d$t$ in Equation 1, as the infinitesimal time d$t$ is an ideal concept and cannot be applied directly in practice. Briefly, assume at time point $t$ the aerosol pH is pH($t$) and sulfate concentration is $SO_4^{2-}(t)$, the newly formed sulfate during the next time step is then $\Delta SO_4^{2-} = P_{SO4}(\mathrm{pH}(t))\,\Delta t$. The new sulfate is $SO_4^{2-}(t + \Delta t) = SO_4^{2-}(t) + \Delta SO_4^{2-}$, while pH($t + \Delta t$) is estimated by ISORROPIA with the new sulfate concentration of $SO_4^{2-}(t + \Delta t)$.

During the calculation, we found that the time interval $\Delta t$ can be important, as a too large $\Delta t$ can lead to over-predictions of sulfates formed within one time step, and thus underestimation in the pH evolutions (Supporting Information S1). Here, we applied a $\Delta t$ of 0.001 s, which was validated to prevent sulfate over-predictions (Supporting Information S1).

#### 2.1.2. Simulation of the Assumed Non-Buffered Aerosols

The pH evolution of the non-buffered aerosols is calculated with a similar iterative method as the buffered system, with the only difference being the pH ∼ $SO_4^{2-}$ relationships. For non-buffered system, we assume that the newly formed sulfate $\Delta SO_4^{2-}$ works like adding sulfuric acid into the system, and thus $[H^+](t + \Delta t) = [H^+](t) + 2\Delta SO_4^{2-}$, namely $\mathrm{pH}(t + \Delta t) = -\lg\left(10^{-\mathrm{pH}(t)} + 2\Delta SO_4^{2-}\right)$.

### 2.2. Estimating the pH Changes Due to Acidification Within 10 s

Another way to evaluate susceptibility of system pH to acidification reactions is to compare the pH changes after a certain time of reactions, for example, 10 s as in Tilgner et al. (2021). To achieve aerosol systems at different

initial pH levels, here we scaled the sulfate concentrations while keeping other conditions the same as the initial setting for NCP scenario (Table S1 in Supporting Information S1) (Cheng et al., 2016; He et al., 2014; Tian et al., 2014; Y. Wang et al., 2014; G. J. Zheng et al., 2015). In that sense, the different initial pH levels actually correspond to different time points following the simulation in Section 2.1, or different degrees during the acidification process of the given aerosol system. A maximum pH of 6.3 can be achieved this way when sulfate concentration is near 0 (Section 2.1). As the pH levels are constrained by the known aerosol compositions, higher pH levels are not available in this simulation. The subsequent pH changes in the next 10 s are then calculated following the iterative calculation methods as described above.

### 2.3. GEOS-Chem Model Simulation

The global GEOS-Chem model simulation was conducted for 2016, and is detailed elsewhere (G. Zheng et al., 2020). The resolution is 2.5° longitude × 2° latitude with 47 vertical layers. The meteorology fields are based on the Modern-Era Retrospective analysis for Research and Applications, Version 2 (MERRA-2) reanalysis meteorological data product (Gelaro et al., 2017) that is updated every 1–3 hr. Anthropogenic emissions were based on the Emission Database for Global Atmospheric Research (EDGAR v4.2) inventory for 2012 (http://edgar.jrc.ec.europa.eu/overview.php?v=42), while updated over China domain with the Multi-resolution Emission Inventory for China inventory (MEIC; http://meicmodel.org) (v1.3) for 2016. Moreover, we have included the international ship emissions for $SO_2$ based on the Arctic Research of the Composition of the Troposphere from Aircraft and Satellites (ARCTAS) inventory (Eyring, Köhler, Lauer, & Lemper, 2005; Eyring, Köhler, van Aardenne, & Lauer, 2005), and that of CO and $NO_x$ based on the International Comprehensive Ocean-Atmosphere Data Set (ICOADS) inventory (C. Wang et al., 2008), and the aircraft $NO_x$ emissions from the Aviation Emissions Inventory Code (AEIC v2.1) inventory (Simone et al., 2013; M. E. J. Stettler et al., 2013; M. E. J. Stettler et al., 2011). Natural source emissions considered include the biomass burning emissions from Global Fire Emissions Database (GFED v4) (van der Werf et al., 2010), biogenic volatile organic compounds and NO emissions calculated by the Model of Emissions of Gases and Aerosols from Nature (MEGAN v2.1) (Guenther et al., 2012), the soil and lightning $NO_x$ emissions (Hudman et al., 2012; Sauvage et al., 2007), and the volcanic $SO_2$ emissions from AeroCom point source data (Carn et al., 2015). While usually run with lower concentration levels, the GEOS-Chem model has been shown to well-reproduce the general spatial and seasonal global distributions of total $NH_3$, $PM_{2.5}$, and thus the aerosol water contents (Bey et al., 2001; Luan & Jaeglé, 2013; G. Luo et al., 2020; M. Luo et al., 2015; Park et al., 2004; Sayer et al., 2010; Shephard et al., 2011; Whitburn et al., 2016; Zeng et al., 2018). See detailed model validations in S. Wang et al. (2020).

## 3. Acidification Versus Multiphase Buffering

Figure 1 shows the simulated acidification process under the NCP scenario upon multiphase oxidation of $SO_2$ (Section 2.1). The acidification rate turns out to be extremely slow, with pH dropping only by 1 unit over ∼9 days of acidification (Figure 1a), comparable with the lifetime of atmospheric fine particles (Seinfeld & Pandis, 2016). Here, we make a conservative assumption with a constant total $NH_3$+$NH_4^+$, while with fast replenishment of $NH_3$ (e.g., a constant $NH_3$(g) as suggested in Weber et al. (Weber et al., 2016)), the acidification could be even slower (Figure S4 and Section S2 in Supporting Information S1). Note that the cases shown in Figure 1 and Figure S4 in Supporting Information S1 here are to demonstrate the effect of acid production on sulfate-forming reactions. Simultaneous change of other species will confuse this effect and was thus turned off for the sake of easy understanding. In reality, all chemical species were subject to emissions, depositions, meteorology and transport processes, etc. (see discussions on Figure 3 below).

As suggested by Zheng et al. (G. Zheng et al., 2020), aerosol pH during severe winter haze conditions in the NCP can be largely buffered by the multiphase buffer agent $NH_4^+/NH_3$. To examine the role of the buffer effect in this slow pH drop, we further calculated the multiphase buffer capacity $\beta$ as (G. Zheng et al., 2020; G. Zheng, Su, Wang, Pozzer, & Cheng, 2022):

$$\beta = 2.303\left(\frac{K_w}{[\mathrm{H}^+(aq)]} + [\mathrm{H}^+(aq)] + \sum_i \frac{K^*_{a,i}[\mathrm{H}^+(\mathrm{aq})]}{(K^*_{a,i} + [\mathrm{H}^+(\mathrm{aq})])^2}[\mathrm{X}_i]^*_{\mathrm{tot}}\right), \text{ for buffered multiphase systems} \quad (2a)$$

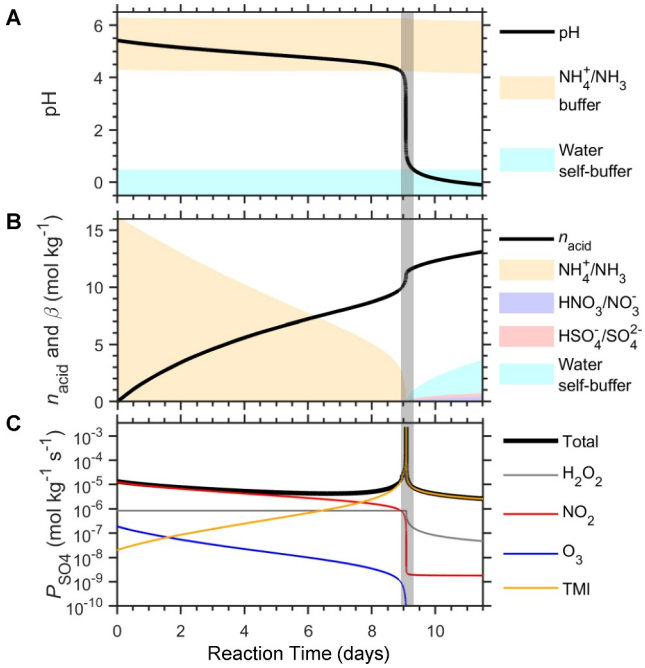


**Figure 1.** Acidification related to sulfate formation under severe haze conditions. Evolution of (a) aerosol pH and the buffered pH ranges (b) the amount of equivalent strong monoacid added to the system ($n_{acid}$) due to the produced sulfates, the buffer capacity $\beta$, and (c) the sulfate production rate ($P_{SO4}$) along the reaction time. The different buffer agents of $NH_4^+/NH_3$, $HNO_3/NO_3^-$, $HSO_4^-/SO_4^{2-}$ and water self-buffering are marked with color shading in (a) and (b). The total $P_{SO4}$ shown in (c) is the sum of the sulfate formation from S(IV) oxidation by $H_2O_2$, $NO_2$, $O_3$ and TMI pathways. Here, we assume a constant total $NH_3$+$NH_4^+$ in the gas-particle system.

where $K_w$ is water dissociation constant, $K_{a,i}$* and $[X_i]_{tot}$* represents the effective acid dissociation constant and total equivalent molality of the buffering agent $X_i$, respectively. The $\beta$ is at its local maximum when pH equals p$K_{a,i}$*. Here all potential buffering agents of $HNO_3/NO_3^-$, $HCl/Cl^-$ and $HSO_4^-/SO_4^{2-}$ are taken into consideration in the $\beta$ calculations (G. Zheng, Su, & Cheng, 2022; Zheng et al., 2023; G. Zheng et al., 2020; G. Zheng, Su, Wang, Pozzer, & Cheng, 2022). Note that for non-buffered aerosol systems, $X_i = 0$ and $\beta$ is:

$$\beta = 2.303\left(K_w/\left[H^+(aq)\right] + \left[H^+(aq)\right]\right), \text{ for non-buffered multiphase systems} \quad (2b)$$

where the remaining terms represent the water self-buffering effect (G. Zheng et al., 2020).

As shown in Figure 1a, the slow acidification in the first ~9 days is attributed to the buffering effect of ammonia, which has a peak buffer pH (i.e., p$K_{a,i}$*) of 5.2, and thus buffers efficiently in the pH range of 5.2 ± 1 (Figure 1a, orange shaded area). For the NCP aerosol system, the initial aerosol pH of 5.4 is close to p$K_{a,i}$*. As the reactions proceed, the accumulated $n_{acid}$ slowly consumes $\beta$ (Figure 1b) and decreases pH. After ~9 days' acidification, nearly all the $\beta$ from ammonia is consumed and pH dropped to the edge of the ammonia buffer range (~4.2). Afterward, in the absence of efficient buffering, pH dropped sharply by 3.7 units (from 4.2 to 0.5) within ~9 hr (the vertical gray shaded area in Figure 1a–1c). When 99% of the ammonia $\beta$ is consumed (i.e., essentially the non-buffered pH ranges of this system), the acidification rate can be particularly high, with pH dropping from 2.9 to 1.3 within 10 min. The enhanced $P_{SO4}$ by the TMI-catalyzed pathway at this pH range also accelerated this breaking-out process (Figure 1c). Especially, because $P_{SO4}$ by the TMI pathway increases with acidity when pH > 2.5, the acidification processes could accelerate itself as it proceeds. When the aerosols are acidified to pH < 2.5, however, $P_{SO4}$ is again suppressed by increasing acidity due to the complex pH-dependence of the $SO_2$-TMI pathway (Figure S1 in Supporting Information S1), and the acidification tends to quench itself. At the low pH range of <0.5, the acidification is slow again, due to both the enhanced water self-buffering effect (Figures 1a and 1b) and the lower $P_{SO4}$ (Figure 1c).

The characteristics of the acidification process discussed above contrast sharply with that estimated for a non-buffered system (black line vs. blue line in Figure 2a; Section 2.2), where the acidification is much quicker. For a wide initial aerosol pH range of 1.5–7, the system is acidified to a relatively stable pH level of ~1.6 (1.4–1.7) within 10 s. Note that our estimation for the non-buffered system (blue line in Figure 2a) is different from that of Tilgner et al. (2021) (dashed gray line in Figure 2a), even after considering the influence of the different $P_{SO4}$ configurations (Section S3 in Supporting Information S1). The large pH drop with increasing initial pH level when it is over ~4.5 of Tilgner et al. (2021) seems unrealistic, as the aerosol pH should be a monotonically decreasing function with reaction time during the acidification process for a given system (Figure 1a; see more discussions Sections S3 and S3 in Supporting Information S1). A pattern like the one in Tilgner et al. (2021) is observed only when an inappropriately large time step *dt* is applied in the iterative calculations, for example, when *dt* equals their total reaction time of 10 s (i.e., only one time step is simulated; Figure S5 in Supporting Information S1). Such a large time step will lead to strong overestimation of the acidification and the unrealistic pH response to the initial pH reported by Tilgner et al. (2021) (Section S3 in Supporting Information S1).

## 4. Reaction Sustainability and Characteristic Buffering Time

The importance of the multiphase buffer effect in stabilizing aerosol acidity is well illustrated by the sharp contrast in acidification processes with versus without the ammonia-buffer effect (Figures 1a and 2a). To describe quantitatively the efficiency of the buffer effect and the time scales of buffering against acidification,

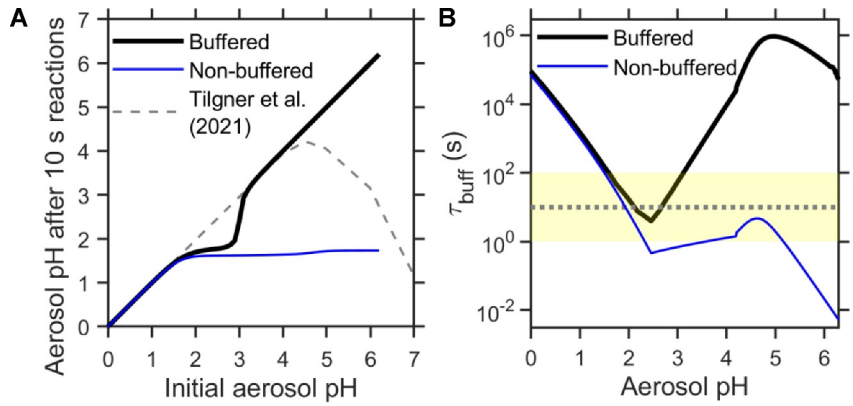


**Figure 2.** Acidification characteristics for buffered and non-buffered aerosols under severe haze conditions. The scenario settings of precursor concentration and production rates are the same as in Figure 1 (Section 2.1, "NCP" scenario in Table S1 of Supporting Information S1) (a) The aerosol pH after 10 s (s) for aerosols with different initial pH levels (b) Characteristic buffering time $\tau_{buff}$. The gray dotted line indicates the reaction time $t_{rct}$ of 10 s as used in (a), while the shaded area indicates the range when $\tau_{buff}$ is comparable with the $t_{rct}$ of 10 s (operationally defined as $0.1\ t_{rct} < \tau_{buff} < 10\ t_{rct}$ here).

we introduce a characteristic buffering time, $\tau_{buff}$, which is defined as the reciprocal of the pH change rate as $\tau_{buff} = |d\text{pH}/dt|^{-1}$. According to the definition of buffer capacity $\beta$ (G. Zheng et al., 2020), that is, the ratio between the amount of acid or base added to the system ($n_{acid}$ or $n_{base}$) and the corresponding pH change ($\beta = -dn_{acid}/d\text{pH}$), it is clear that the efficiency of the multiphase buffer effect against acidification is intrinsically connected with the buffer capacity. We can thus derive the acidification rate ($d\text{pH}/dt$) and $\tau_{buff}$ as:

$$d\text{pH}/dt = (-dn_{acid}/\beta)/dt = (-dn_{acid}/dt)/\beta = -2P_{SO4}/\beta \quad (3)$$

$$\tau_{buff} = |d\text{pH}/dt|^{-1} = 0.5\ \beta/P_{SO4} \quad (4)$$

While in deriving Equations 3 and 4 only the sulfate acidifying effect is considered, the above analysis can be easily extended to more general acidifying processes like the production of $HNO_3$ or HCl, etc., as (see detailed deduction in Supporting Information S1 Section S4.1):

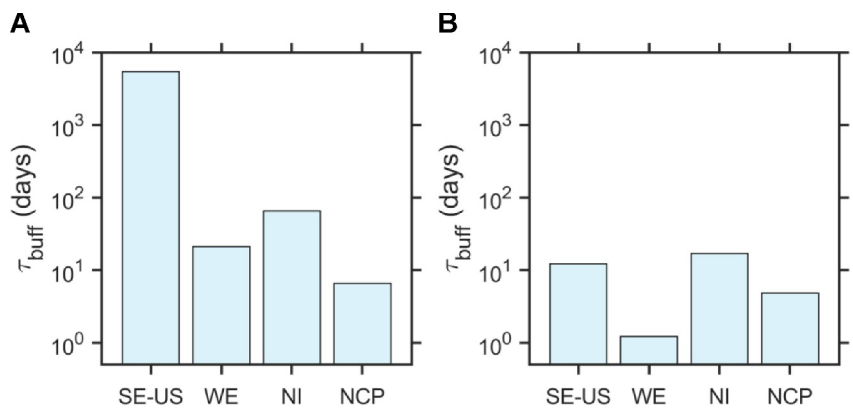


**Figure 3.** Observation-based estimations of characteristic buffering time, $\tau_{buff}$, under different ambient conditions. The scenarios shown are characteristic for the Southeastern USA (SE-US), western Europe (WE), northern India (NI), and the North China Plain (NCP) (see scenario settings in Table S1 of Supporting Information S1). Note that the $\tau_{buff}$ values shown here correspond to different time periods (see Table S1 in Supporting Information S1). Only sulfate formation from the multiphase reactions in aerosol waters are considered in (a), while sulfate formation due to the $SO_2$ oxidation in the gas-phase by OH radicals is included in (b).

$$\tau_{buff} = |d\mathrm{pH}/dt|^{-1} = \beta/\sum_i \nu_i P_{acid,i} \quad (5)$$

where $P_{acid,i}$ is the production rate of acidic species $i$, and $\nu_i$ is the stoichiometric number of $H^+$ associated with the corresponding acid. For example, for sulfate-generating reactions, the corresponding acid is $H_2SO_4$ and $\nu$ is 2; while $\nu$ is 1 for nitrate-generating reactions. For instance, when both sulfate and nitrate is produced, the acidification would accelerate with a lower $\tau_{buff}$ of:

$$\tau_{buff} = |d\mathrm{pH}/dt|^{-1} = \beta/(2\,P_{SO4} + P_{NO3}) \quad (6)$$

Assuming a nitrate production rate similar to that of sulfate, the total $P_{acid}$ would increase by 1.5 times and the $\tau_{buff}$ would decrease by 1/3, which would not influence the order-of-magnitude of $\tau_{buff}$. Thus for $\tau_{buff}$ of days, the conclusion that the aerosol pH and its related processes like sulfate productions can be sustained still holds.

Here, $\tau_{buff}$ represents the sustainability of the buffering effect (including the water self-buffer effect) for a given system against the acidifying reactions. $\tau_{buff}$ is a property of the aerosol system, which is determined by aerosol and gases compositions through Equations 2 and 4. When $\tau_{buff}$ is much larger than the reaction time $t_{rct}$, the buffering effect dominates over the acidifying effect, and the aerosol pH can be sustained. When $\tau_{buff} << t_{rct}$, the acidifying effect overwhelms the buffering effect, and a quick pH drop is expected. Take the NCP scenario with a reaction time $t_{rct} = 10$ s for illustration (Figure 2a). For the buffered system, $\tau_{buff} >> t_{rct}$ (operationally defined as $\tau_{buff} > 10\,t_{rct}$ here) when pH < 1.6 or pH > 3.2 (Figure 2b, black line), and therefore the aerosol pH changes little ($\Delta$pH < 0.1) within these two ranges (Figure 2a, black line). In comparison, for the non-buffered system, $\tau_{buff} >> t_{rct}$ is satisfied only when pH < 1.6, and the acidification is obvious ($\Delta$pH > 0.1) for any initial pH level above this value. The detailed principles and the quantified relationship of how $\tau_{buff}$ can be used to characterize the time needed to reach a certain $\Delta$pH, or to predict the $\Delta$pH (or final pH) after a certain reaction time $t_{rct}$, are discussed Section S4 and Figures S6–S7 in Supporting Information S1.

## 5. Global Distribution of Buffering Time Scale

The above analysis of $\tau_{buff}$ under the NCP scenario can be extended to other ammonia-buffered atmospheric aerosol systems, based on ambient observations and global simulations. To address the wide concern that whether the acidification due to multiphase reactions would quench the high-pH favored reactions (Angle et al., 2021; Chen et al., 2022; Tilgner et al., 2021; W. Wang et al., 2021), we calculated $\tau_{buff}$ for the multiphase reactions exclusively (Figures 3a and 4a). Figure 3a shows the $\tau_{buff}$ of sulfate formation under different ambient conditions, characteristic for the Southeastern USA (SE-US), the North China Plain (NCP), northern India (NI), and western Europe (WE) (see scenario settings in Table S1 of Supporting Information S1) (Behera & Sharma, 2010; Bencs et al., 2008; Cheng et al., 2016; Guo et al., 2017; He et al., 2014; Tian et al., 2014; Y. Wang et al., 2014; G. Zheng et al., 2020; G. J. Zheng et al., 2015). Under the conditions observed in these regions, the corresponding $\tau_{buff}$ for the four scenarios are all above 1 day. The shortest $\tau_{buff}$ is observed for the NCP scenario, considering the higher precursor concentrations and higher reaction rates (Table S1 in Supporting Information S1). Figure 4a further compares the global distribution of $\tau_{buff}$ for the ammonia-buffered regions, with site-specific reactant concentrations and aerosol pH levels based on GEOS-Chem simulations (Section 2.3). Here the ammonia-buffered region is determined by the criteria that the difference between system pH and buffer peak of ammonia, $pK_a^{*,ni}$ of $NH_3$, is within $\pm$1.3 unit, or when the $NH_3(g)/NH_4^+(p)$ gas-particle partitioning ratio is within 1/20 to 20. The definition is discussed in G. Zheng et al. (2023), which is a further improvement of the previous definition (G. Zheng et al., 2020). In agreement with the observation-based estimations (Figure 3a), globally, $\tau_{buff}$ is generally on the order of 10 days or months, with smaller $\tau_{buff}$ found in the most polluted regions like northern China and India. Note that while $\tau_{buff}$ was shown in ammonia-buffered regions only (Figure 4), the contribution of other buffer pairs like $HNO_3/NO_3^-$ are already taken into consideration, as implied in the definition of $\beta$ (Equation 2a). In agreement with our previous studies (G. Zheng, Su & Cheng et al., 2022; G. Zheng et al., 2023; G. Zheng et al., 2020; G. Zheng, Su, Wang, Pozzer, & Cheng, 2022), for most of the continental urban areas, the ammonia is the dominant buffering agent (Figure 4c). Here, the contribution of ammonia buffering effect to total buffer capacity is calculated at the actual pH levels for each grid (calculation method detailed in (G. Zheng et al., 2020; G. Zheng et al., 2023)), which is less than the maximum buffer capacity of ammonia.

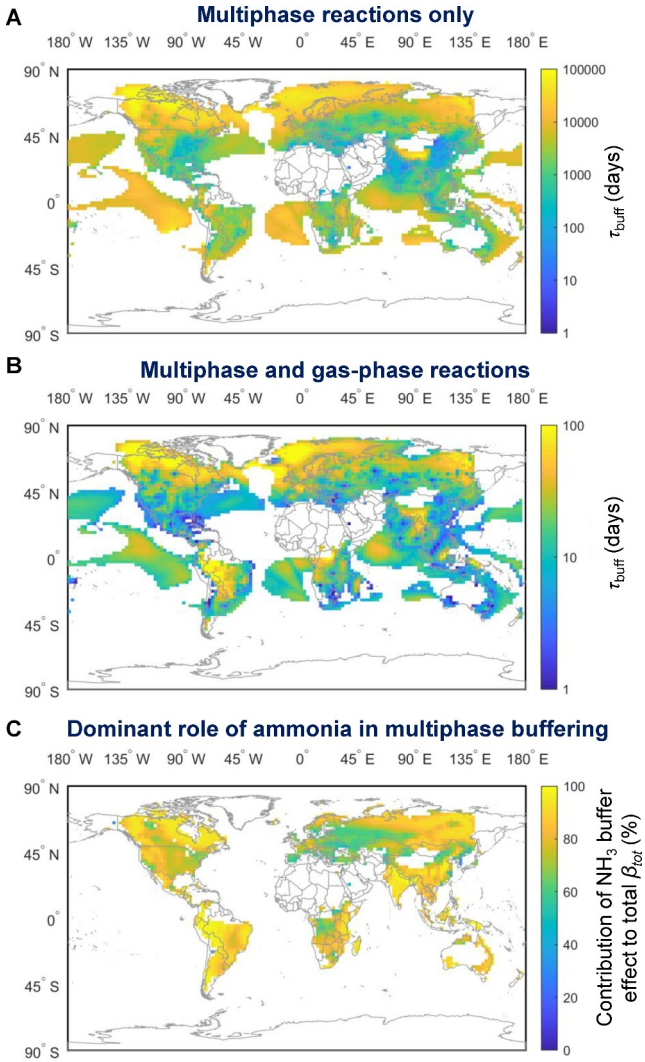


**Figure 4.** Global distribution of characteristic buffering time, $\tau_{buff}$, for ammonia-buffered regions upon sulfate formations. The $\tau_{buff}$ is estimated with site-specific annual average reactant concentrations and aerosol pH levels based on GEOS-Chem simulations in 2016 (Section 2.3). Only sulfate formation from the multiphase reactions in aerosol waters are considered in (a), while sulfate formation due to the $SO_2$ oxidation in the gas-phase by OH radicals is included in (b). Here, only results of the surface regions are shown, while the $\tau_{buff}$ is also applicable in upper layers as long as aerosol pH can be calculated (c) Contribution of $NH_4^+/NH_3$ multiphase buffer effect to total buffer capacity. Here the contribution is calculated at the actual pH levels for each grid; see detailed calculation method elsewhere (G. Zheng, Su & Cheng et al., 2022; G. Zheng, Su, Wang, Pozzer, & Cheng, 2022).

Acidic species generated by gas-phase reactions, however, can also condense onto the particles, contributing to the acidification process. Figures 3b and 4b further consider the influence of the major gas phase $H_2SO_4$ formation pathway by $SO_2$ and OH radical reactions (Cheng et al., 2016; Seinfeld & Pandis, 2016). Based on ambient observations (Figures 3a and 4a), this influence is extremely large for the cleaner scenarios of SE-US and WE, reducing $\tau_{buff}$ by 1∼2 orders of magnitude. In comparison, the influence on the more polluted scenarios of NI and NCP is much lower, reducing $\tau_{buff}$ only by 3.9 and 1.4 times, respectively. This confirms that globally, gas-phase oxidation of $SO_2$ is one of the most important sources of sulfate, while multiphase reactions play an important role under polluted haze conditions with high aerosol concentrations and high precursor concentrations, such as the NCP and NI scenarios (Figure S8 in Supporting Information S1) (Cheng et al., 2016; G. Zheng et al., 2020; G. J. Zheng et al., 2015). However, even considering the gas phase chemistry, the $\tau_{buff}$ in the buffered regime is still on the scale of days, suggesting the importance of the multiphase buffer effect in resisting extremely quick acidification, which would otherwise have occurred in minutes.

The results based on global simulations also supported this conclusion (Figure 4b), with $\tau_{buff}$ on scale of days for all multiphase buffered regions, in terms of annual averages (Figure 4) and each season alike (Figure S9 in Supporting Information S1). The $\tau_{buff}$ is also susceptible to ammonia emissions, with higher ammonia emissions correspond to higher buffer capacity β and therefore larger $\tau_{buff}$ (Equation 5; Supporting Information S1). Previous studies have indicated up to ∼40% bias in the ammonia emission inventories as constrained by nitrogen deposition, etc., and the bias may have some seasonality (L. Liu et al., 2022; Q. Zhang et al., 2019; X. Zhang et al., 2017). Nevertheless, $a$ ±40% fluctuations in ammonia would result in $\tau_{buff}$ variations at roughly the same extent, which would not influence the order of magnitude of $\tau_{buff}$. It also shows that over most areas, there is a sharp (∼2 orders of magnitude) decrease of $\tau_{buff}$ when gas-phase reactions are included (Figure 4a). This indicates that in terms of the global budget, except for in-cloud production, the sulfate formation in most regions is still dominated by the gas-phase oxidation of $SO_2$, and the multiphase phase production of sulfate in aerosol water will mainly contribute under polluted conditions (Cheng et al., 2016; Tao et al., 2020).

The multiphase buffering effect is important in sustaining a stable aerosol pH and thus a stable reaction rate of pH-sensitive reactions. Depending on the relationship of aerosol acidity and reaction rates, multiphase reactions can be classified into self-amplifying, self-quenching, or weakly-dependent. In a non-buffered system, the self-amplification would proceed quickly, and the self-quenching reactions will be shut down promptly (Figures 5a and 5b). Under buffered conditions, however, the buffer effect can hinder the propagation of self-amplifying reactions, or sustain the self-quenching reactions (Figures 5c and 5d).

## 6. Conclusions

Our results show that the ammonia multiphase buffering effect is important in sustaining a stable aerosol pH and enhancing the overall sulfate production, thereby impacting the global sulfate burden and haze formation. Both the $SO_2$-$O_3$ and $SO_2$-$NO_2$ reactions are self-quenching. In a non-buffered marine environment, the self-quenching $SO_2$-$O_3$ reaction on sea salt aerosols can quickly shut down on a scale of minutes (Figures 5a and 5b) (Alexander et al., 2005; Angle et al., 2021; Seinfeld & Pandis, 2016). However, in ammonia-buffered polluted continental regions and marine regions receiving $NH_3$ from continental sources (Figure 4), the self-quenching sulfate

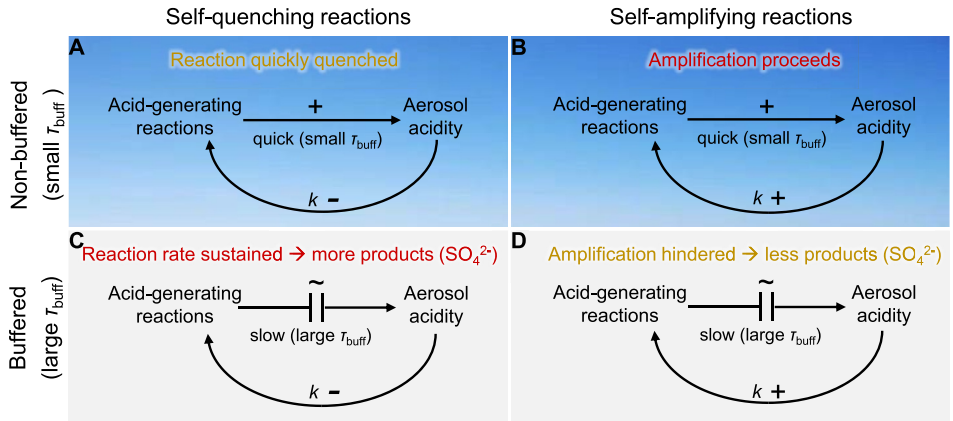


**Figure 5.** Influence of acidification versus the multiphase buffer effect on multiphase reactions. The left panels (a, c) and the right panels (b, d) are for self-quenching reactions and self-amplifying reactions, respectively. The upper panels (a, b) and the lower panels (c, d) are for non-buffered and buffered systems, respectively. Here, $k$ is the reaction rate, and $\tau_{buff}$ is the characteristic buffering time. The acid-generating reactions will increase aerosol acidity, while this increase is obvious only when the reaction time is comparable with the $\tau_{buff}$. The resultant acidity changes would in turn influence the acid generation rates $k$. In a non-buffered system with small $\tau_{buff}$ (a, b), such feedback loops are quick, and the acid-generating reactions will be quickly quench or amplified. In a buffered system with large $\tau_{buff}$ (c, d), however, the acidity adjusts slowly with the generated acids, and the acid-generating reactions can be sustained at stable rates.

formation reactions of $SO_2$-$O_3$ and $SO_2$-$NO_2$ can be sustained over days, contributing significantly to sulfate production during haze formation (Figure 5c) (Cheng et al., 2016), as illustrated above. Even for the partially self-amplifying $SO_2$-TMI reaction, the overall sulfate yield is higher with multiphase buffering. The $SO_2$-TMI reaction would turn from self-amplifying to self-quenching when pH drops below ∼2.5 for the NCP scenario (Figure 1; Figure S1 in Supporting Information S1). Under non-buffered conditions, this rapid acidification would quickly drop the pH to the turnover point, followed by a rapid quenching (Figure 1). Therefore, the overall sulfate yield would be smaller than under buffered conditions over a time scale of ∼1 hr. In addition to sulfate production, the stability of aerosol acidity could also influence the production of other components like secondary organics, and the estimation in nitrogen depositions, etc (Carlton et al., 2010; Franco et al., 2021; Hallquist et al., 2009; Jang et al., 2002; Surratt et al., 2007).

The characteristic buffering time $\tau_{buff}$ provided a scientific metric on how long the acidity of aerosols in a multiphase system can be maintained. This is essential for understanding the of atmospheric acidification and pH-dependent chemical reactions and for time-step optimization in chemical transport models. For example, when $\tau_{buff}$ is much larger than the time step of the present model $\tau_0$ (i.e., $\tau_{buff} >> \tau_0$), pH can be calculated with current time step setting; while a small $\tau_{buff}$ would require reducing $\tau_0$ (see more discussions in Supporting Information S5 (A. J. Ding et al., 2016; Shi et al., 2017)). The large $\tau_{buff}$ as shown in this study resolve the debate about the importance of different sulfate-forming multiphase reactions, and further highlights the pervasive influence of anthropogenic ammonia emissions in shaping chemical environments and controlling the dominant reaction pathways in the atmosphere. The $\tau_{buff}$ is not limited to sulfate production and can also be used for other introduction of acidic or alkaline compounds (e.g., nitric acid/nitrate etc.). Moreover, $\tau_{buff}$ is not limited to atmospheric acidification. Similar concepts of characteristic buffering time can also be introduced for ocean acidification, and even go beyond the acid-base buffering and to different kind of buffering effects in the Earth system, for example, the buffer effect of seawater on atmospheric $CO_2$ (E. Liao et al., 2021; Yi et al., 2001) or the buffering mechanisms of cloud and precipitation responses to aerosol perturbations (Stevens & Feingold, 2009), etc. The $\tau_{buff}$ is not limited to sulfate production, and can also be used for any introduction of acidic or alkaline compounds (e.g., nitric acid/nitrate etc.). Moreover, $\tau_{buff}$ is not limited to atmospheric acidification. Similar concepts of characteristic buffering time can also be introduced for ocean acidification, and even go beyond the acid-base buffering and to any kind of buffering effect in the Earth system, for example, the buffer effect of seawater on atmospheric $CO_2$ (E. Liao et al., 2021; Yi et al., 2001) or the buffering mechanisms of cloud and precipitation responses to aerosol perturbations (Stevens & Feingold, 2009), etc.

## Conflict of Interest

The authors declare no conflicts of interest relevant to this study.

## Data Availability Statement

Key data used is available at: Zheng, G. J. (2024). Characteristic buffering time against sulfate acidification [Dataset]. Zenodo. https://doi.org/10.5281/zenodo.12608976. Other data used in the analysis are provided in Table S1 of Supporting Information S1. Relative codes for buffer capacity calculations are provided in our previous work (G. Zheng et al., 2020; G. Zheng, Su & Cheng et al., 2022; G. Zheng, Su, Wang, Pozzer, & Cheng, 2022). The calculation of multiphase effective acid dissociation constant is given in (G. Zheng et al., 2020). The non-ideality parameterization code is given in (G. Zheng, Su & Cheng et al., 2022; G. Zheng, Su, Wang, Pozzer, & Cheng, 2022). Calculation for the contribution of a given buffer agent to the total buffer capacity at the given system pH is given in (G. Zheng, Su & Cheng et al., 2022; G. Zheng, Su & Wang et al.,. 2022; G. Zheng et al., 2023).

**Acknowledgments**
This study is support by Max Planck Society (MPG). Y.C. would like to thank the Minerva Program of MPG. G. Z. acknowledges the National Natural Science Foundation of China (22188102). H.S. thanks the Strategy Priority Research Program of Chinese Academy of Sciences (XDB0760000), Chinese Academy of Sciences President's International Fellowship Initiative (2024PG0014) and the National Key Scientific and Technological Infrastructure Project "Earth System Science Numerical Simulator Facility".

## References

Akimoto, H., & Hirokawa, J. (2020). *Atmospheric multiphase chemistry: Fundamentals of secondary aerosol formation*. John Wiley and Sons.

Alexander, B., Park, R. J., Jacob, D. J., Li, Q. B., Yantosca, R. M., Savarino, J., et al. (2005). Sulfate formation in sea-salt aerosols: Constraints from oxygen isotopes. *Journal of Geophysical Research*, *110*(D10). https://doi.org/10.1029/2004JD005659

Angle, K. J., Crocker, D. R., Simpson, R. M. C., Mayer, K. J., Garofalo, L. A., Moore, A. N., et al. (2021). Acidity across the interface from the ocean surface to sea spray aerosol. *Proceedings of the National Academy of Sciences*, *118*(2), e2018397118. https://doi.org/10.1073/pnas.2018397118

Behera, S. N., & Sharma, M. (2010). Investigating the potential role of ammonia in ion chemistry of fine particulate matter formation for an urban environment. *The Science of the Total Environment*, *408*(17), 3569–3575. https://doi.org/10.1016/j.scitotenv.2010.04.017

Bencs, L., Ravindra, K., de Hoog, J., Rasoazanany, E. O., Deutsch, F., Bleux, N., et al. (2008). Mass and ionic composition of atmospheric fine particles over Belgium and their relation with gaseous air pollutants. *Journal of Environmental Monitoring*, *10*(10), 1148–1157. https://doi.org/10.1039/b805157g

Bey, I., Jacob, D. J., Yantosca, R. M., Logan, J. A., Field, B. D., Fiore, A. M., et al. (2001). Global modeling of tropospheric chemistry with assimilated meteorology: Model description and evaluation. *Journal of Geophysical Research*, *106*(D19), 23073–23095. https://doi.org/10.1029/2001JD000807

Carlton, A. G., Bhave, P. V., Napelenok, S. L., Edney, E. O., Sarwar, G., Pinder, R. W., et al. (2010). Model representation of secondary organic aerosol in CMAQv4.7. *Environmental Science and Technology*, *44*(22), 8553–8560. https://doi.org/10.1021/es100636q

Carn, S. A., Yang, K., Prata, A. J., & Krotkov, N. A. (2015). Extending the long-term record of volcanic $SO_2$ emissions with the ozone mapping and profiler suite nadir mapper. *Geophysical Research Letters*, *42*(3), 925–932. https://doi.org/10.1002/2014gl062437

Chameides, W. L., & Stelson, A. W. (1992). Aqueous-phase chemical processes in deliquescent sea-salt aerosols: A mechanism that couples the atmospheric cycles of S and sea salt. *Journal of Geophysical Research*, *97*(D18), 20565–20580. https://doi.org/10.1029/92JD01923

Chen, Z., Liu, P., Wang, W., Cao, X., Liu, Y.-X., Zhang, Y.-H., & Ge, M. (2022). Rapid sulfate formation via uncatalyzed autoxidation of sulfur dioxide in aerosol microdroplets. *Environmental Science and Technology*, *56*(12), 7637–7646. https://doi.org/10.1021/acs.est.2c00112

Cheng, Y., Zheng, G., Wei, C., Mu, Q., Zheng, B., Wang, Z., et al. (2016). Reactive nitrogen chemistry in aerosol water as a source of sulfate during haze events in China. *Science Advances*, *2*(12), e1601530. https://doi.org/10.1126/sciadv.1601530

Ding, A. J., Huang, X., Nie, W., Sun, J. N., Kerminen, V. M., Petaja, T., et al. (2016). Enhanced haze pollution by black carbon in megacities in China. *Geophysical Research Letters*, *43*(6), 2873–2879. https://doi.org/10.1002/2016gl067745

Ding, J., Zhao, P., Su, J., Dong, Q., Du, X., & Zhang, Y. (2019). Aerosol pH and its driving factors in Beijing. *Atmospheric Chemistry and Physics*, *19*(12), 7939–7954. https://doi.org/10.5194/acp-19-7939-2019

Eyring, V., Köhler, H. W., Lauer, A., & Lemper, B. (2005a). Emissions from international shipping: 2. Impact of future technologies on scenarios until 2050. *Journal of Geophysical Research*, *110*(D17), D17306. https://doi.org/10.1029/2004jd005620

Eyring, V., Köhler, H. W., van Aardenne, J., & Lauer, A. (2005b). Emissions from international shipping: 1. The last 50 years. *Journal of Geophysical Research*, *110*(D17), D17305. https://doi.org/10.1029/2004jd005619

Fountoukis, C., & Nenes, A. (2007). Isorropia II: A computationally efficient thermodynamic equilibrium model for $K^+$-$Ca^{2+}$-$Mg^{2+}$-$NH_4^+$-$Na^+$-$SO_4^{2-}$-$NO_3^-$-$Cl^-$-$H_2O$ aerosols. *Atmospheric Chemistry and Physics*, *7*(17), 4639–4659. https://doi.org/10.5194/acp-7-4639-2007

Franco, B., Blumenstock, T., Cho, C., Clarisse, L., Clerbaux, C., Coheur, P. F., et al. (2021). Ubiquitous atmospheric production of organic acids mediated by cloud droplets. *Nature*, *593*(7858), 233–237. https://doi.org/10.1038/s41586-021-03462-x

Gelaro, R., McCarty, W., Suárez, M. J., Todling, R., Molod, A., Takacs, L., et al. (2017). The Modern-Era Retrospective analysis for Research and Applications, version 2 (MERRA-2). *Journal of Climate*, *30*(14), 5419–5454. https://doi.org/10.1175/jcli-d-16-0758.1

Guenther, A. B., Jiang, X., Heald, C. L., Sakulyanontvittaya, T., Duhl, T., Emmons, L. K., & Wang, X. (2012). The model of emissions of gases and aerosols from nature version 2.1 (MEGAN2.1): An extended and updated framework for modeling biogenic emissions. *Geoscientific Model Development*, *5*(6), 1471–1492. https://doi.org/10.5194/gmd-5-1471-2012

Guo, H., Weber, R. J., & Nenes, A. (2017). High levels of ammonia do not raise fine particle pH sufficiently to yield nitrogen oxide-dominated sulfate production. *Scientific Reports*, *7*(1), 12109. https://doi.org/10.1038/s41598-017-11704-0

Hallquist, M., Wenger, J. C., Baltensperger, U., Rudich, Y., Simpson, D., Claeys, M., et al. (2009). The formation, properties and impact of secondary organic aerosol: Current and emerging issues. *Atmospheric Chemistry and Physics*, *9*(14), 5155–5236. https://doi.org/10.5194/acp-9-5155-2009

He, H., Wang, Y., Ma, Q., Ma, J., Chu, B., Ji, D., et al. (2014). Mineral dust and NOx promote the conversion of SO2 to sulfate in heavy pollution days. *Scientific Reports*, *4*(1), 4172. https://doi.org/10.1038/srep04172

Hudman, R. C., Moore, N. E., Mebust, A. K., Martin, R. V., Russell, A. R., Valin, L. C., & Cohen, R. C. (2012). Steps towards a mechanistic model of global soil nitric oxide emissions: Implementation and space based-constraints. *Atmospheric Chemistry and Physics*, *12*(16), 7779–7795. https://doi.org/10.5194/acp-12-7779-2012

Jang, M., Czoschke, N. M., Lee, S., & Kamens, R. M. (2002). Heterogeneous atmospheric aerosol production by acid-catalyzed particle-phase reactions. *Science*, *298*(5594), 814–817. https://doi.org/10.1126/science.1075798

Keene, W. C., Sander, R., Pszenny, A. A. P., Vogt, R., Crutzen, P. J., & Galloway, J. N. (1998). Aerosol pH in the marine boundary layer: A review and model evaluation. *Journal of Aerosol Science*, *29*(3), 339–356. https://doi.org/10.1016/S0021-8502(97)10011-8

Laskin, A., Gaspar, D. J., Wang, W., Hunt, S. W., Cowin, J. P., Colson, S. D., & Finlayson-Pitts, B. J. (2003). Reactions at interfaces as a source of sulfate formation in sea-salt particles. *Science*, *301*(5631), 340–344. https://doi.org/10.1126/science.1085374

Liao, E., Resplandy, L., Liu, J., & Bowman, K. W. (2021). Future weakening of the ENSO ocean carbon buffer under anthropogenic forcing. *Geophysical Research Letters*, *48*(18), e2021GL094021. https://doi.org/10.1029/2021GL094021

Liao, H., Seinfeld, J. H., Adams, P. J., & Mickley, L. J. (2004). Global radiative forcing of coupled tropospheric ozone and aerosols in a unified general circulation model. *Journal of Geophysical Research*, *109*(D16). https://doi.org/10.1029/2003JD004456

Liu, L., Xu, W., Lu, X., Zhong, B., Guo, Y., Lu, X., et al. (2022). Exploring global changes in agricultural ammonia emissions and their contribution to nitrogen deposition since 1980. *Proceedings of the National Academy of Sciences*, *119*(14), e2121998119. https://doi.org/10.1073/pnas.2121998119

Liu, T., & Abbatt, J. P. D. (2021). Oxidation of sulfur dioxide by nitrogen dioxide accelerated at the interface of deliquesced aerosol particles. *Nature Chemistry*, *13*(12), 1173–1177. https://doi.org/10.1038/s41557-021-00777-0

Liu, T., Chan, A. W. H., & Abbatt, J. P. D. (2021). Multiphase oxidation of sulfur dioxide in aerosol particles: Implications for sulfate formation in polluted environments. *Environmental Science and Technology*, *55*(8), 4227–4242. https://doi.org/10.1021/acs.est.0c06496

Liu, T., Clegg, S. L., & Abbatt, J. P. D. (2020). *Fast oxidation of sulfur dioxide by hydrogen peroxide in deliquesced aerosol particles*. Proceedings of the National Academy of Sciences. https://doi.org/10.1073/pnas.1916401117.201916401.

Luan, Y., & Jaeglé, L. (2013). Composite study of aerosol export events from East Asia and North America. *Atmospheric Chemistry and Physics*, *13*(3), 1221–1242. https://doi.org/10.5194/acp-13-1221-2013

Luo, G., Yu, F., & Moch, J. M. (2020). Further improvement of wet process treatments in GEOS-Chem v12.6.0: Impact on global distributions of aerosol precursors and aerosols. *Geoscientific Model Development Discussions*, *2020*, 1–39. https://doi.org/10.5194/gmd-2020-11

Luo, M., Shephard, M. W., Cady-Pereira, K. E., Henze, D. K., Zhu, L., Bash, J. O., et al. (2015). Satellite observations of tropospheric ammonia and carbon monoxide: Global distributions, regional correlations and comparisons to model simulations. *Atmospheric Environment*, *106*, 262–277. https://doi.org/10.1016/j.atmosenv.2015.02.007

Park, R. J., Jacob, D. J., Field, B. D., Yantosca, R. M., & Chin, M. (2004). Natural and transboundary pollution influences on sulfate-nitrate-ammonium aerosols in the United States: Implications for policy. *Journal of Geophysical Research*, *109*(D15). https://doi.org/10.1029/2003JD004473

Pye, H. O. T., Nenes, A., Alexander, B., Ault, A. P., Barth, M. C., Clegg, S. L., et al. (2020). The acidity of atmospheric particles and clouds. *Atmospheric Chemistry and Physics*, *20*(8), 4809–4888. https://doi.org/10.5194/acp-20-4809-2020

Salter, M. E., Hamacher-Barth, E., Leck, C., Werner, J., Johnson, C. M., Riipinen, I., et al. (2016). Calcium enrichment in sea spray aerosol particles. *Geophysical Research Letters*, *43*(15), 8277–8285. https://doi.org/10.1002/2016GL070275

Sauvage, B., Martin, R. V., van Donkelaar, A., Liu, X., Chance, K., Jaeglé, L., et al. (2007). Remote sensed and in situ constraints on processes affecting tropical tropospheric ozone. *Atmospheric Chemistry and Physics*, *7*(3), 815–838. https://doi.org/10.5194/acp-7-815-2007

Sayer, A. M., Thomas, G. E., Palmer, P. I., & Grainger, R. G. (2010). Some implications of sampling choices on comparisons between satellite and model aerosol optical depth fields. *Atmospheric Chemistry and Physics*, *10*(22), 10705–10716. https://doi.org/10.5194/acp-10-10705-2010

Seinfeld, J. H., & Pandis, S. N. (2016). *Atmospheric chemistry and physics: From air pollution to climate change*. John Wiley and Sons.

Shephard, M. W., Cady-Pereira, K. E., Luo, M., Henze, D. K., Pinder, R. W., Walker, J. T., et al. (2011). TES ammonia retrieval strategy and global observations of the spatial and seasonal variability of ammonia. *Atmospheric Chemistry and Physics*, *11*(20), 10743–10763. https://doi.org/10.5194/acp-11-10743-2011

Shi, G., Xu, J., Peng, X., Xiao, Z., Chen, K., Tian, Y., et al. (2017). pH of aerosols in a polluted atmosphere: Source contributions to highly acidic aerosol. *Environmental Science and Technology*, *51*(8), 4289–4296. https://doi.org/10.1021/acs.est.6b05736

Simone, N. W., Stettler, M. E. J., & Barrett, S. R. H. (2013). Rapid estimation of global civil aviation emissions with uncertainty quantification. *Transportation Research Part D: Transport and Environment*, *25*, 33–41. https://doi.org/10.1016/j.trd.2013.07.001

Snider, G., Weagle, C. L., Murdymootoo, K. K., Ring, A., Ritchie, Y., Stone, E., et al. (2016). Variation in global chemical composition of PM2.5: Emerging results from SPARTAN. *Atmospheric Chemistry and Physics*, *16*(15), 9629–9653. https://doi.org/10.5194/acp-16-9629-2016

Stettler, M. E. J., Boies, A. M., Petzold, A., & Barrett, S. R. H. (2013). Global civil aviation black carbon emissions. *Environmental Science and Technology*, *47*(18), 10397–10404. https://doi.org/10.1021/es401356v

Stettler, M. E. J., Eastham, S., & Barrett, S. R. H. (2011). Air quality and public health impacts of UK airports. Part I: Emissions. *Atmospheric Environment*, *45*(31), 5415–5424. https://doi.org/10.1016/j.atmosenv.2011.07.012

Stevens, B., & Feingold, G. (2009). Untangling aerosol effects on clouds and precipitation in a buffered system. *Nature*, *461*(7264), 607–613. https://doi.org/10.1038/nature08281

Su, H., Cheng, Y., & Pöschl, U. (2020). New multiphase chemical processes influencing atmospheric aerosols, air quality, and climate in the anthropocene. *Accounts of Chemical Research*, *53*(10), 2034–2043. https://doi.org/10.1021/acs.accounts.0c00246

Surratt, J. D., Lewandowski, M., Offenberg, J. H., Jaoui, M., Kleindienst, T. E., Edney, E. O., & Seinfeld, J. H. (2007). Effect of acidity on secondary organic aerosol formation from isoprene. *Environmental Science and Technology*, *41*(15), 5363–5369. https://doi.org/10.1021/es0704176

Tao, W., Su, H., Zheng, G., Wang, J., Wei, C., Liu, L., et al. (2020). Aerosol pH and chemical regimes of sulfate formation in aerosol water during winter haze in the North China Plain. *Atmospheric Chemistry and Physics*, *20*(20), 11729–11746. https://doi.org/10.5194/acp-20-11729-2020

Tian, S., Pan, Y., Liu, Z., Wen, T., & Wang, Y. (2014). Size-resolved aerosol chemical analysis of extreme haze pollution events during early 2013 in urban Beijing, China. *Journal of Hazardous Materials*, *279*, 452–460. https://doi.org/10.1016/j.jhazmat.2014.07.023

Tilgner, A., Schaefer, T., Alexander, B., Barth, M., Collett Jr, J. L., Fahey, K. M., et al. (2021). Acidity and the multiphase chemistry of atmospheric aqueous particles and clouds. *Atmospheric Chemistry and Physics*, *21*(17), 13483–13536. https://doi.org/10.5194/acp-21-13483-2021

van der Werf, G. R., Randerson, J. T., Giglio, L., Collatz, G. J., Mu, M., Kasibhatla, P. S., et al. (2010). Global fire emissions and the contribution of deforestation, savanna, forest, agricultural, and peat fires (1997–2009). *Atmospheric Chemistry and Physics*, *10*(23), 11707–11735. https://doi.org/10.5194/acp-10-11707-2010

Wang, C., Corbett, J. J., & Firestone, J. (2008). Improving spatial representation of global ship emissions inventories. *Environmental Science and Technology*, *42*(1), 193–199. https://doi.org/10.1021/es0700799

Wang, S., Su, H., Chen, C., Tao, W., Streets, D. G., Lu, Z., et al. (2020). Natural gas shortages during the "coal-to-gas" transition in China have caused a large redistribution of air pollution in winter 2017. *Proceedings of the National Academy of Sciences*, *117*(49), 31018–31025. https://doi.org/10.1073/pnas.2007513117

Wang, W., Liu, M., Wang, T., Song, Y., Zhou, L., Cao, J., et al. (2021). Sulfate formation is dominated by manganese-catalyzed oxidation of $SO_2$ on aerosol surfaces during haze events. *Nature Communications*, *12*(1), 1993. https://doi.org/10.1038/s41467-021-22091-6

Wang, Y., Yao, L., Wang, L., Liu, Z., Ji, D., Tang, G., et al. (2014). Mechanism for the formation of the January 2013 heavy haze pollution episode over central and eastern China. *Science China Earth Sciences*, *57*(1), 14–25. https://doi.org/10.1007/s11430-013-4773-4

Weber, R. J., Guo, H., Russell, A. G., & Nenes, A. (2016). High aerosol acidity despite declining atmospheric sulfate concentrations over the past 15 years. *Nature Geoscience*, *9*(4), 282–285. https://doi.org/10.1038/ngeo2665

Whitburn, S., Van Damme, M., Clarisse, L., Bauduin, S., Heald, C. L., Hadji-Lazaro, J., et al. (2016). A flexible and robust neural network IASI-NH3 retrieval algorithm. *Journal of Geophysical Research: Atmospheres*, *121*(11), 6581–6599. https://doi.org/10.1002/2016jd024828

Yi, C., Gong, P., Xu, M., & Qi, Y. (2001). The effects of buffer and temperature feedback on the oceanic uptake of $CO_2$. *Geophysical Research Letters*, *28*(5), 751–754. https://doi.org/10.1029/2000GL011569

Zeng, Y., Tian, S., & Pan, Y. (2018). Revealing the sources of atmospheric ammonia: A review. *Current Pollution Reports*, *4*(3), 189–197. https://doi.org/10.1007/s40726-018-0096-6

Zhang, Q., Pan, Y., He, Y., Zhao, Y., Zhu, L., Zhang, X., et al. (2019). Bias in ammonia emission inventory and implications on emission control of nitrogen oxides over North China Plain. *Atmospheric Environment*, *214*, 116869. https://doi.org/10.1016/j.atmosenv.2019.116869

Zhang, X., Wu, Y., Liu, X., Reis, S., Jin, J., Dragosits, U., et al. (2017). Ammonia emissions may be substantially underestimated in China. *Environmental Science and Technology*, *51*(21), 12089–12096. https://doi.org/10.1021/acs.est.7b02171

Zheng, G., Su, H., & Cheng, Y. (2022a). Revisiting the key driving processes of the decadal trend of aerosol acidity in the U.S. *ACS Environmental Au*, *2*(4), 346–353. https://doi.org/10.1021/acsenvironau.1c00055

Zheng, G., Su, H., & Cheng, Y. (2023). Role of carbon dioxide, ammonia, and organic acids in buffering atmospheric acidity: The distinct contribution in clouds and aerosols. *Environmental Science and Technology*, *57*(34), 12571–12582. https://doi.org/10.1021/acs.est.2c09851

Zheng, G., Su, H., Wang, S., Andreae, M. O., Pöschl, U., & Cheng, Y. (2020). Multiphase buffer theory explains contrasts in atmospheric aerosol acidity. *Science*, *369*(6509), 1374–1377. https://doi.org/10.1126/science.aba3719

Zheng, G., Su, H., Wang, S., Pozzer, A., & Cheng, Y. (2022b). Impact of non-ideality on reconstructing spatial and temporal variations in aerosol acidity with multiphase buffer theory. *Atmospheric Chemistry and Physics*, *22*(1), 47–63. https://doi.org/10.5194/acp-22-47-2022

Zheng, G. J. (2024). Characteristic buffering time against sulfate acidification [Dataset]. *Zenodo*. https://doi.org/10.5281/zenodo.12608976

Zheng, G. J., Duan, F. K., Su, H., Ma, Y. L., Cheng, Y., Zheng, B., et al. (2015). Exploring the severe winter haze in Beijing: The impact of synoptic weather, regional transport and heterogeneous reactions. *Atmospheric Chemistry and Physics*, *15*(6), 2969–2983. https://doi.org/10.5194/acp-15-2969-2015